
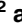




# Phasin interactome reveals the interplay of PhaF with the polyhydroxyalkanoate transcriptional regulatory protein PhaD in *Pseudomonas putida*

Natalia A. Tarazona <sup>1†</sup>, Ana M. Hernández-Arriaga <sup>1,2</sup>, Ryan Kniewel <sup>1,2</sup> and M. Auxiliadora Prieto <sup>1,2\*</sup>

<sup>1</sup>Polymer Biotechnology Group, Department of Microbial and Plant Biotechnology, Centro de Investigaciones Biológicas Margarita Salas, Consejo Superior de Investigaciones Científicas (CIB-CSIC), Madrid, 28040, Spain.

<sup>2</sup>Interdisciplinary Platform for Sustainable Plastics Towards a Circular Economy-CSIC (SusPlast-CSIC), Spain.

## Summary

**Phasin PhaF, a multifunctional protein associated with the surface of polyhydroxyalkanoate (PHA) granules that also interacts with the nucleoid, contributes significantly to PHA biogenesis in pseudomonads. As a protein present on the surface of PHA granules, PhaF participates in granule stabilization and segregation, whereas its deletion has a notable impact on overall transcriptome, PHA accumulation and cell physiology, suggesting more extensive functions besides solely being a granule structural protein. Here, we followed a systematic approach to detect potential interactions of PhaF with other components of the cell, which could pinpoint unexplored functions of PhaF in the regulation of PHA production. We determined the PhaF interactome in *Pseudomonas putida* KT2440 via pull-down-mass spectrometry (PD-MS) experiments. PhaF complexed with PHA-related proteins, phasin Phal and the transcriptional regulator PhaD, interactions that were verified to be direct using *in vivo* two-hybrid analysis. The determination of the PHA granule proteome showed that Phal and three other potential PhaF interacting partners, but not PhaD, were granule-associated**

**proteins. Analysis of the interaction of PhaF and PhaD with the *phaI* promoter by EMSA suggested a new role for PhaF in interacting with PhaD and raises new questions on the regulatory system controlling *pha* gene expression.**

## Introduction

Polyhydroxyalkanoates (PHA) are biodegradable polyesters synthesized from (*R*)-3-hydroxyacyl-CoA monomers, which can be produced from intermediates of carbon metabolism by diverse microorganisms and accumulate as intracellular insoluble granules (termed PHA granules or carbonosomes) (Rehm, 2010; Prieto *et al.*, 2016). Phasins are multifunctional proteins with the ability to associate to the surface of PHA granules *in vivo* and to PHA beads or films *in vitro* (Jendrossek, 2009; Maestro and Sanz, 2017; Tarazona *et al.*, 2019b). Although the exact composition of the carbonosome is unknown, phasins are recognized as the predominant granule associated proteins (GAPs) and make up approximately 2% of the total granule mass (Wieczorek *et al.*, 1995; Sznajder *et al.*, 2015). These low molecular weight proteins are present in all known PHA-accumulating bacteria and are produced synchronized with PHA synthesis and play key roles in PHA metabolism (York *et al.*, 2002; Mozejko-Ciesielska and Serafim, 2019). Generally, two main roles for phasins have been assigned: (i) To prevent the aggregation of PHA granules (coalescence), regulating the number and size of carbonosomes. (ii) To inhibit nonspecific attachment of other proteins or hydrophobic molecules to PHA granules (Mezzina and Pettinari, 2016; Maestro and Sanz, 2017). Other roles have been assigned to phasins depending on the microorganism and the metabolic state of the cell. For instance, pseudomonad phasin PhaF functions to distribute and segregate the granules to daughter cells during cell division that is proposed to be through simultaneous bridging of PHA to the nucleoid. Moreover, its deletion impacts the transcriptome of the cell including transcription of the *pha* cluster in *Pseudomonas putida* (see below) (Galán *et al.*, 2011).

Received 20 May, 2020; revised 16 July, 2020; accepted 21 July, 2020. \*For correspondence. E-mail auxi@cib.csic.es and natalia.tarazona@gmail.com; Tel: 34-918373112(ext.4228); Fax: 34-915360432. †Present address: Institute of Biomaterial Science, Helmholtz-Zentrum Geesthacht, Teltow, Germany.

PhaF is one of the most abundant proteins produced during PHA accumulating conditions in *P. putida* KT2440 (de Eugenio *et al.*, 2010; Mozejko-Ciesielska and Serafim, 2019). This bacterium produces medium chain length poly 3-*R*-hydroxyalkanoates (mcl-PHA, comprised of repeating units with 6–14 carbon atoms) with the machinery encoded by the *pha* gene cluster that contains two divergently transcribed operons. The *phaC1ZC2D* operon encodes two synthases (or polymerases, PhaC1 and PhaC2), a depolymerase (PhaZ) and the PhaD transcriptional regulator (Huisman *et al.*, 1991). The *phaIF* operon is located downstream of *phaC1ZC2D* and codes for the phasins PhaF and PhaI (Prieto *et al.*, 1999). This *pha* cluster is well-conserved among mcl-PHA producing pseudomonads (Fig. 1).

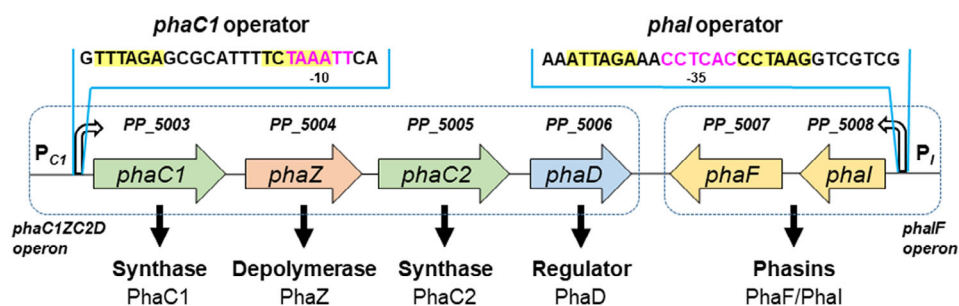
The accumulation of PHA in *Pseudomonas* is subject to extensive regulation at different levels, at the transcriptional and posttranscriptional level by specific and global regulatory factors, and through regulation of carbon flux through different pathways that provide PHA precursors (Prieto *et al.*, 2016; Kniewel *et al.*, 2019). Translational fusions with a *lacZ* reporter gene demonstrated that the *pha* locus in *P. putida* contains five functional promoters located upstream of the *phaC1*, *phaZ*, *phaC2*, *phaF* and *phaI* genes (denoted  $P_{C1}$ ,  $P_Z$ ,  $P_{C2}$ ,  $P_F$  and  $P_I$ ), suggesting the co-existence of a variety of polycistronic transcription units (de Eugenio *et al.*, 2010).  $P_{C1}$  and  $P_I$  seem to be the most active promoters of the *pha* cluster, allowing the transcription of both operons (Fig. 1). At the transcriptional level, it was demonstrated that the two operons, *phaC1ZC2D* and *phaIF*, are under the partial control of the regulator protein PhaD, which belongs to the TetR family of transcriptional regulators (de Eugenio *et al.*, 2010). This family comprises one-component signal transduction systems in bacteria in which a single polypeptide contains both a signal-sensing domain and a DNA-binding domain (Cuthbertson and Nodwell, 2013). Unlike most characterized members of this family, PhaD functions as an activator and not as a repressor of

transcription (de Eugenio *et al.*, 2010; Cuthbertson and Nodwell, 2013). PhaD binds to a 25 and 29 bp operator region of the  $P_{C1}$  and  $P_I$  promoters, respectively, and is proposed to bind a CoA intermediate of fatty acid  $\beta$ -oxidation (de Eugenio *et al.*, 2010). However, the true effector of PhaD remains uncertain.

The involvement of PhaF in the transcriptional regulation of the *pha* gene cluster was first presumed in *P. putida* GPo1 (Prieto *et al.*, 1999). Later, the disruption of the *phaF* gene in *P. putida* KT2442, was shown to affect PHA production (1.5-fold reduction) and the transcription of the *phaC1* and *phaI* genes (Galán *et al.*, 2011). The transcription level of *phaC1* decreased approximately 3.5-fold with respect to wild type and *phaI* reached its highest transcriptional level much later in stationary phase. Even though there is no evidence for the specific binding of PhaF to the promoter regions of *pha* genes, preliminary transcriptomic analyses of a *phaF* mutant strain suggested an indirect regulatory effect on the expression of these genes as shown by the slight downregulation of the *pha* cluster (Galán *et al.*, 2011).

A wider effect on the *P. putida* *phaF* mutant transcriptome has also been observed, including upregulation of acetyl-CoA acetyltransferase (UniProt Q88E32), a key enzyme in fatty acid degradation, and other proteins involved in metabolic and regulatory processes (Galán *et al.*, 2011). However, the regulatory function of PhaF during PHA synthesis in *Pseudomonas* species is not fully understood.

The multifunctional nature of phasin PhaF is related to its modular characteristics. It is an intrinsically disordered protein composed of three motifs. An amino terminal region that interacts with PHA, a carboxy terminal containing a motif capable of binding DNA in a sequence non-specific manner (Galán *et al.*, 2011; Maestro *et al.*, 2013), and a central core that contains a leucine zipper motif responsible for its homo- and hetero-oligomerization, as recently demonstrated with PhaI, the other phasin in *P. putida* (Tarazona *et al.*, 2019a). Here, we



**Fig. 1.** Diagram of the *pha* cluster in *P. putida* KT2440. The *pha* cluster contains two divergently transcribed operons (dashed boxes), *phaC1ZC2D* and *phaIF*. Both operons are under the control of the regulator PhaD, which functions as an activator of transcription. The PhaD operators are 25 bp in the  $P_{C1}$  promoter and 29 bp in the  $P_I$  promoter. Both sequences contain a single binding site formed by inverted half sites of 6 bp (highlighted nucleotides) separated by 8 bp. The  $-35$  and  $-10$  boxes contained in the promoters are shown in magenta. [Color figure can be viewed at [wileyonlinelibrary.com](http://wileyonlinelibrary.com)]

followed a systematic approach at the proteomic level to detect other potential interacting partners of PhaF, which could pinpoint unexplored functions of this phasin in the regulation of PHA. We used an affinity pull-down mass spectrometry (PD-MS) technique to screen for proteins that interact with PhaF. Promising interacting partners were cross-validated with proteins determined to be part of the PHA granule proteome to evaluate their impact on PhaF function. The determination of PhaD as a PhaF interactor was further substantiated using *in vivo* and *in vitro* techniques to validate protein–protein and protein–DNA interactions.

## Results

### Identification of PhaF interaction partners

The multi-modular structure of phasin PhaF and the observation that it plays roles in several cellular processes suggests that interactions occur between this protein and other components. To test this hypothesis, we designed an *in vitro* interaction/pull-down experiment combined with mass spectrometry (PD-MS) (Supplemental Fig. S1A). In consideration of the reported sequence non-specific binding of PhaF to DNA through its carboxy terminal domain (Galán *et al.*, 2011), the homogenate was treated with DNase and the soluble fraction was separated by centrifugation (Supplemental Fig. S1B). This was done to reduce the non-specific association of DNA bound proteins with PhaF, and thus increase the accuracy of identified proteins. Moreover, the presence of any PHA granules would impede proper binding of His<sub>6</sub>-PhaF complexes to the Ni-Sepharose column. Therefore, the PHA granule fraction was also removed from the homogenate by centrifugation. However, we cannot exclude the presence of some GAPs in the isolated soluble fraction. The DNA- and PHA-depleted soluble fraction used for PD-MS is shown in Supplemental Fig. S1B, lane 1. To identify non-specific interacting proteins, the *P. putida* soluble fraction alone (no PhaF added) was passed through a clean Ni-Sepharose column and processed in the same manner as the sample. Proteins identified in this preparation by MS were deemed background and were removed from the final analysis.

To validate the PD-MS experiments, an anti-Phal western blot was performed (Fig. 2A), relying on the reported direct interaction between PhaF and Phal (Tarazona *et al.*, 2019a). Western blot analysis revealed a single band with a molecular weight of approximately 17 kDa, confirming Phal as a PhaF interacting partner and the suitability of the experimental design.

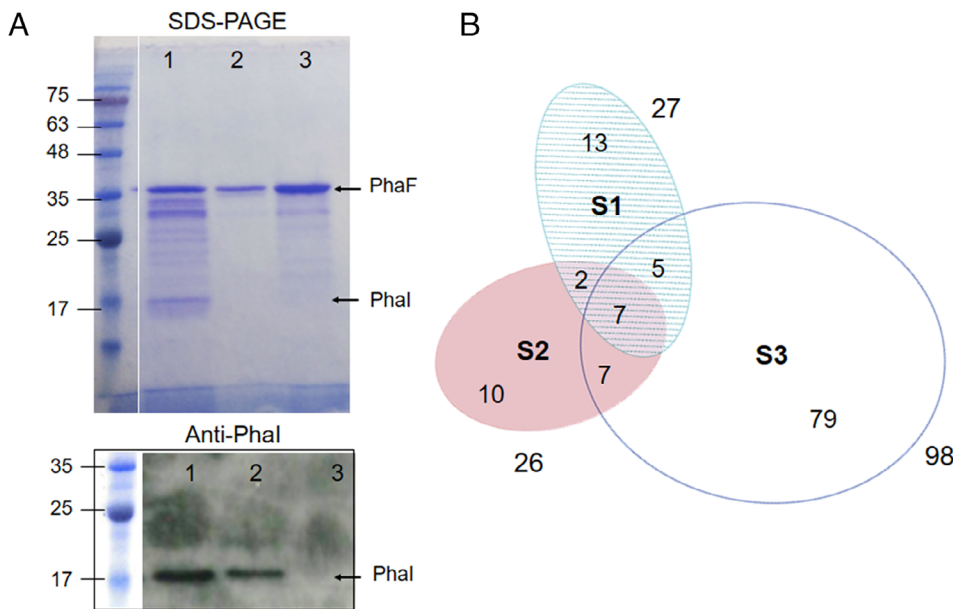
For MS analyses, the polyacrylamide gel containing the His<sub>6</sub>-PhaF co-eluted protein fraction (example in

Supplemental Fig. S1C, lanes 1 and 2) and the fraction containing proteins non-specifically bound to the column alone, NC (Supplemental Fig. S1C, lane 3) were run approximately 1 cm, cut, subjected to trypsin digestion and analysed by MS, as described in Experimental Procedures.

Three or four proteins, respectively, were found to bind non-specifically to the column in the two negative control samples (NC) and were considered to be background (data not shown). None of these seven proteins were detected to be present in any of the three His<sub>6</sub>-PhaF bound complex biological replicates (S1, S2 and S3) analysed. This could be attributed to the high concentration of His<sub>6</sub>-PhaF saturating binding sites in the column, thereby preventing the binding of other non-specifically interacting proteins.

Figure 2B compares the number of proteins identified as captured by His<sub>6</sub>-PhaF in the three biological replicates (S1, S2 and S3). Samples S1 and S2 identified nearly the same number of proteins, 27 and 26, respectively, where 9 of these proteins are common in both samples. In the case of S3, a higher number of proteins were found (98). From these, 12 and 14 proteins were also detected in S1 and S2, respectively. The higher outcome in S3 could be explained by a higher concentration of His<sub>6</sub>-PhaF bait in the fraction recovered following the washing steps and the elution of the complexes (as shown in Table 1). This difference notwithstanding, a high level of reproducibility between all three replicates was supported by correlation coefficients greater than 0.999 for all pairwise comparisons of proteins common in all three datasets (Pearson's *r*). However, around 62% of the detected proteins in the S3 sample generated only a single peptide spectrum match (PSM), which represents the total number of identified peptide spectra matched for a given protein. Therefore, these proteins are likely false positive interactions brought about by a high level of His<sub>6</sub>-PhaF bait in this sample. When two or more PSMs was set as the threshold for protein identification, the number of proteins found in S3 was reduced to 48, compared to 10 for both S1 and S2.

If only proteins detected in all the three replicates were considered, the PD-MS experiments suggested seven potential PhaF interacting proteins (Fig. 2B, Table 1). In decreasing number of PSMs averaged across the replicates, the proteins captured by PhaF were: phasin Phal (58 PSMs), ATP synthase subunit beta (21 PSMs), TetR-like transcriptional regulator PhaD (18 PSMs), tRNA methyltransferase TrmJ (17 PSMs), putative electron transfer flavoprotein-ubiquinone oxidoreductase (16 PSMs) and outer membrane protein OprF (11 PSMs). The highest PSM value corresponded to PhaF (3082), likely due to the presence of high quantities of bait protein and its self-oligomerization (Tarazona *et al.*, 2019a).



**Fig. 2.** PhaF pull-down and mass spectrometry.

A. 12.5% SDS-PAGE of pull-down eluted fractions (Coomassie stained, upper panel), and anti-Phal western blot (lower panel). Lanes 1 and 2, His<sub>6</sub>-PhaF with soluble protein fraction of *P. putida* eluted first with 265 mM (lane 1), and then with 500 mM imidazole (lane 2), for removal of residual complexes; lane 3, purified recombinant His<sub>6</sub>-PhaF.

B. Area-proportional Venn diagram indicating the number of proteins identified in the PD-MS experiments using His<sub>6</sub>-PhaF as bait. S1, S2 and S3 represent biological replicates. The total number of proteins identified in S1, S2 and S3 were 27, 26 and 98, respectively. PhaF is one of the seven proteins common in all three replicates. [Color figure can be viewed at [wileyonlinelibrary.com](http://wileyonlinelibrary.com)]

**Table 1.** Proteins associated with PhaF identified by MALDI-TOF mass spectrometry.

UniProt	Protein	Score <sup>a</sup>			Coverage <sup>b</sup> %			# Peptides <sup>c</sup>			# PSM <sup>d</sup>		
		S1	S2	S3	S1	S2	S3	S1	S2	S3	S1	S2	S3
Q88D21	Phasin PhaF	2919	2929	4013	90	92	93	39	37	41	913	921	1248
Q88D20	Phasin PhaI	78	73	65	70	68	50	14	11	10	22	20	16
Q88D22	TetR family transcriptional regulator, PhaD	26	10	24	42	19	14	5	3	2	9	3	6
Q88PL1	tRNA (cytidine/uridine-2'-O)-methyltransferase, TrmJ	18	16	31	17	17	22	3	3	3	6	5	6
Q88F95	Putative electron transfer flavoprotein	12	3	38	5	4	19	2	1	8	4	1	11
Q88BX4	ATP synthase subunit beta	7	8	73	7	7	43	2	2	12	2	2	17
Q88L46	Outer membrane protein, OprF	4	6	36	6	8	29	1	2	5	1	2	8

<sup>a</sup>Sum of the ion scores of all peptides that were identified for each protein.

<sup>b</sup>Percentage of the protein sequence covered by identified peptides.

<sup>c</sup>Number of distinct peptides identified in the protein.

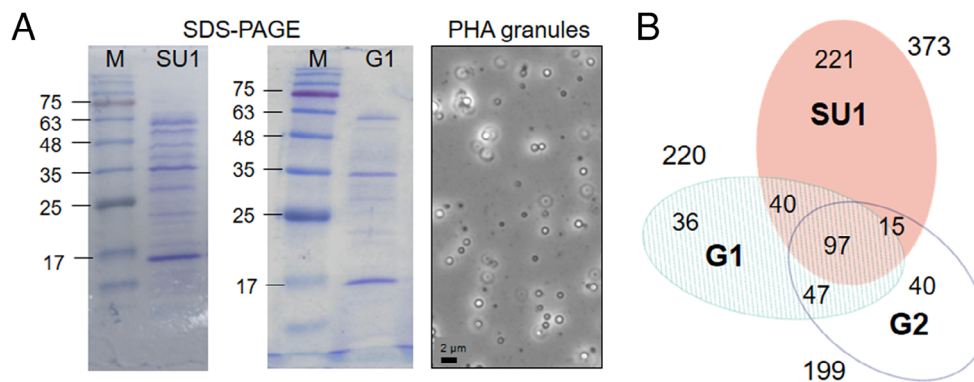
<sup>d</sup>Number of Peptide Spectrum Matches, indicating the total number of identified peptide spectra matched for the protein.

### Proteomic analysis of PHA carbonosomes

PhaF is one of the most abundant proteins on the PHA granule surface. In fact, a recent study on the proteomic responses of *P. putida* to nutrient limitation during PHA synthesis revealed that PhaF was the only protein from the *pha* cluster with a significant increase in concentration during PHA accumulation (Mozejko-Ciesielska and Serafim, 2019). To confirm if the interaction of PhaF with the six PhaF-interacting partners identified by PD-MS were present on the granule surface, a proteomic analysis of isolated PHA granules was carried out. PHA granules were prepared using two different centrifugation separation methods with glycerol or sucrose (Fig. 3A). In total, three granule fractions were made, two biological replicates resulting from the glycerol gradient method, G1

and G2; and one replicate from the sucrose gradient, SU1. Lysates from cells grown to accumulate PHA used for the G1 and G2 granule preparations were treated with DNase, while the lysate for the SU1 granule preparation was not treated. The glycerol or sucrose PHA granule fractions were analysed by MS as described for the PD-MS experiment.

To ensure the strictest methodology for identifying PHA granule-associated proteins, we applied the following workflow. First, a threshold of two or more PSMs was set for individual samples. Around 200 proteins were identified in either of the G1 and G2 (glycerol gradient) PHA granule preparations (Fig. 3B). These two datasets had a high degree of correlation, with a correlation coefficient of 0.760 (Pearson's *r*). Moreover, 373 proteins were



**Fig. 3.** Analysis of PHA granule proteome.

A. Coomassie stained 12.5% SDS-PAGE of *P. putida* PHA granules obtained using either sucrose (SU1) or glycerol (G1) gradient methods. Phase contrast micrograph of purified granules from sample SU1. M, molecular weight markers.

B. Area-proportional Venn diagram of MS datasets for the number of proteins identified in the granule preparations using a glycerol gradient (G1 and G2) or a sucrose gradient (SU1). The total number of proteins identified in SU1, G1 and G2 were 373, 220 and 199, respectively. [Color figure can be viewed at [wileyonlinelibrary.com](http://wileyonlinelibrary.com)]

identified in the SU1 sucrose gradient preparation. When the methodologies to isolate the granules were compared, G1 versus SU1 or G2 versus SU1, a smaller, yet positive correlation was present, with correlation coefficients of 0.313 and 0.422, respectively (Pearson's  $r$ ). The decreased correlation between the glycerol and sucrose preparations was likely due to the removal of DNA from the G1 and G2 samples, which was not done for the SU1 preparation, and led to the identification of nearly twice the number of proteins. For the second step in the analysis workflow, only the proteins detected in all three samples were taken into account, resulting in 97 putative granule-associated proteins. Finally, only proteins identified by at least two distinct peptides were included (not to be confused with the PSM values). The 78 curated proteins are listed in Supplemental Table S1.

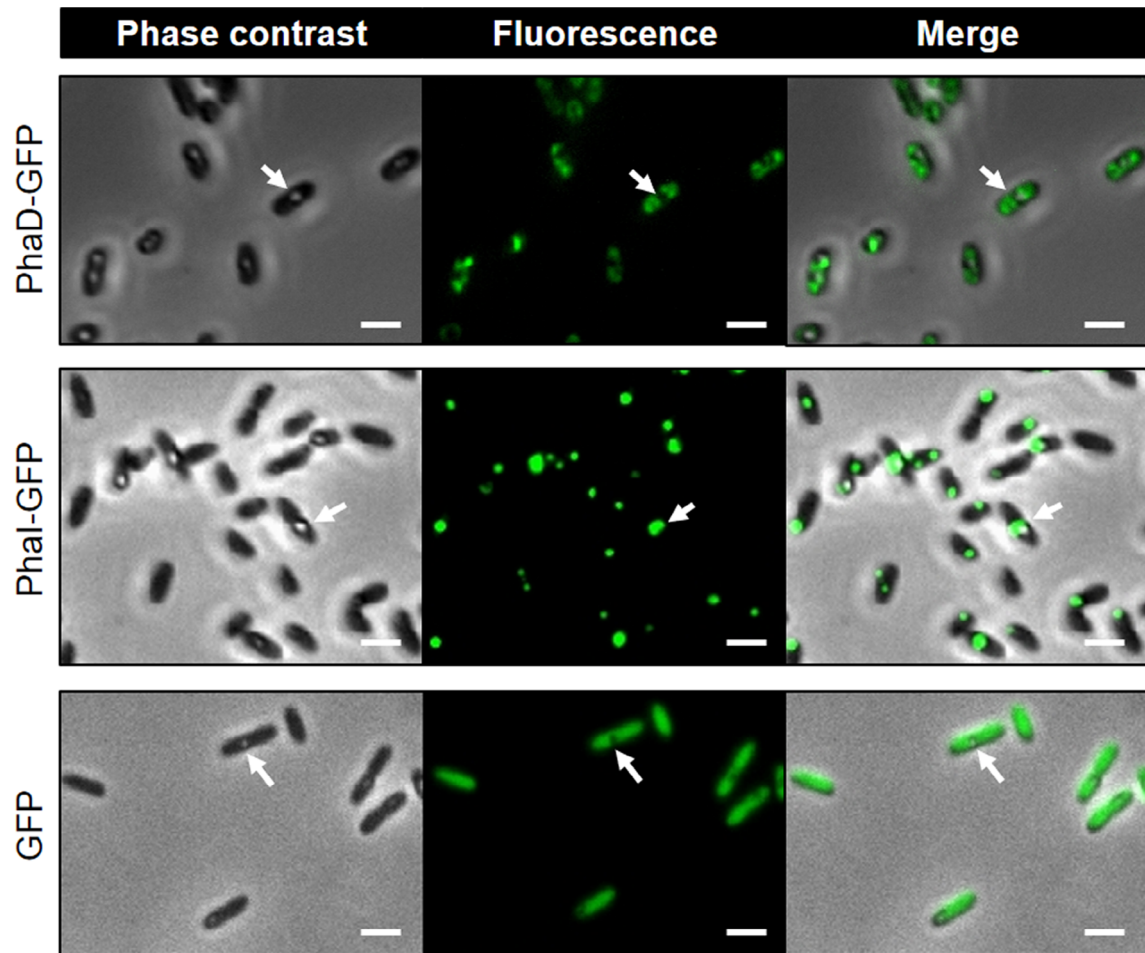
Although the procedure for PHA granule isolation and the bioinformatic analysis were quite stringent, several proteins without obvious involvement in PHA metabolism were found associated with granules Supplemental Table S1. They mostly included abundant cellular constituents classified as ATPase subunits, proteins involved in transcription and translation, cell periphery, transport and outer membrane proteins, and protein folding-associated proteins or chaperones. The significance of detecting these proteins is examined further in the Discussion. However, some of the most abundant proteins found are known to be associated with PHA granules in pseudomonads. These include phasins PhaF and PhaI and synthases PhaC1 and PhaC2 from the *pha* cluster, as well as the acyl-CoA synthase FadD1 (Q88EB7). FadD1 plays a central role in the mobilization of PHA, as it converts 3-hydroxycarboxylic acid monomers, obtained by PhaZ-mediated degradation of PHA, to 3-hydroxyacyl-CoA (3HA-CoA) (Ruth *et al.*, 2008). Remarkably, other fatty acid metabolism-related proteins including FabG

(Q88QB3), FadE (Q88LN6), FadL (Q88M85) and a putative acyl-CoA dehydrogenase (Q88QW6) were also identified. The association of these proteins with PHA granules should be validated, but are not further addressed herein.

The remaining two proteins of the *pha* cluster, the depolymerase PhaZ and the transcriptional regulator PhaD, were not found when the restrictions were applied to the proteomic analysis. For instance, only one peptide from PhaD (corresponding to a single PSM) was detected in the glycerol gradient sample G2; and PhaZ was detected in two of the three samples analysed (two PSMs and one peptide in G1; plus four PSMs and three peptides in SU1). However, this might be due to the very low production of these proteins during PHA accumulation as PhaZ was previously found to be associated with PHA granules (de Eugenio *et al.*, 2007; de Eugenio *et al.*, 2010). The fact that PhaD interacted with PhaF, but it was not found on the granule surface would indicate that the interaction between these two proteins is not involved in PhaF's role in the formation and stabilization of PHA granules.

#### Subcellular localization of PhaD

As PhaD was found to interact with PhaF in the PD-MS experiments, yet was not detected as part of the granule proteome, we sought to validate this result *in vivo* and to determine where PhaD was located in PHA producing cells. *P. putida* cells carrying plasmids induced to express a PhaD-GFP fusion (pSEVA238-DG) or a PhaI-GFP fusion (pSEVA238-IG) were visualized microscopically following growth in PHA production conditions. Bacteria expressing the PhaD-GFP fusion showed a fluorescence pattern inconsistent with PHA granules as it was dissimilar to the location of granules indicated by PhaI-GFP (Fig. 4). The PhaD-GFP fluorescence pattern was also distinct



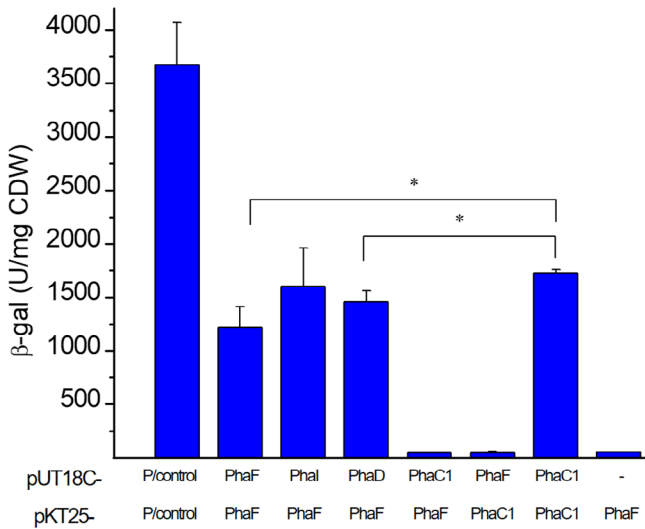
**Fig. 4.** Fluorescent microscopy of *P. putida* expressing GFP fusion proteins. *P. putida* cells carrying the plasmids expressing the PhaD-GFP fusion (pSEVA238-DG), the PhaI-GFP fusion (pSEVA238-IG), or GFP alone (pSEVA238-G). The fluorescence of the GFP constructs was analysed in PHA production cultures following a 2 h induction with 3-methylbenzoate. White bars represent 2  $\mu$ m and white arrows indicate PHA granules. [Color figure can be viewed at [wileyonlinelibrary.com](http://wileyonlinelibrary.com)]

from that of GFP expressed alone, which was found to be uniformly distributed throughout the cytoplasm. This uniform distribution pattern was not observed in either of the previous fusion proteins suggesting that the presence of GFP did not alter their localization. Instead, the PhaD-GFP fusion showed a fluorescence pattern more consistent with proteins associated with nucleoid and ribosomes in *P. putida* during PHA production as described before for GFP-tagged RpoC ( $\beta'$  subunit of RNA polymerase) and GFP-tagged L13 (50S ribosomal protein) (Kim *et al.*, 2019).

#### *PhaF and PhaD interact directly in vivo in a heterologous system*

From the PD-MS results, we showed that PhaF not only interacts with PhaI, as previously demonstrated, but also interacts *in vitro* with PhaD (Tarazona *et al.*, 2019a). To

confirm a direct physical interaction *in vivo* between PhaF and PhaD, we used bacterial two-hybrid analysis (detailed in Experimental Procedures). *E. coli* co-expressing the T18-PhaD and T25-PhaF complementation fragment fusions showed levels of  $\beta$ -galactosidase activity more than 20 times the negative control plasmids (Figs. 5, 1460 U/mg cell dry weight (CDW) versus 52 U/mg CDW). This value was similar to the  $\beta$ -galactosidase results detected for the homo-oligomerization of T18-PhaF and T25-PhaF (1218 U/mg CDW) or the interaction of T18-PhaI and T25-PhaF (1600 U/mg CDW). This indicated that a strong interaction between PhaF and PhaD occurs *in vivo* that was not required to be mediated by other *P. putida* proteins, such as PhaI. The interaction of PhaF with the synthase PhaC1 was also tested to confirm if the absence of detection of PhaC1 in the PD-MS results was due to the lack of PhaC1 in the soluble fraction, or if PhaF and PhaC1 are definitively not



**Fig. 5.** PhaF and PhaD interaction by bacterial two-hybrid assay.  $\beta$ -galactosidase activities (Miller Units per mg of cell dry weight, U/mg CDW) of *E. coli* BTH101 cells co-transformed with different combinations of the complementary pUT18C target and pUT25 bait plasmids, expressing PhaF, PhaI, PhaD or PhaC1. The values correspond to the average obtained from three transformant clones tested for each interaction with error bars showing standard deviations. Control corresponds to leucine zipper constructs as a positive interaction control. The rightmost column utilized the negative control pUT18C empty vector along with pKT25-*phaF*. Statistically significant differences between the samples ( $p$  values <0.05) are marked with an asterisk. [Color figure can be viewed at [wileyonlinelibrary.com](http://wileyonlinelibrary.com)]

capable of interacting. Only a background level  $\beta$ -galactosidase activity was detected from the interaction between T18-PhaC1 and T25-PhaF (44 U/mg CDW), providing experimental evidence for the lack of a direct interaction between these two GAPs. The specificity of the results was confirmed by the fact that PhaF expressed from plasmid pKT25-*phaF* did not lead to significant  $\beta$ -galactosidase activity when tested with the complementary empty plasmid pKT25 (52 U/mg CDW). We also confirmed that PhaC1 formed dimers when tested by the two-hybrid assay (1727 U/mg CDW), as has been demonstrated for other PHA synthases, and further confirms the correct expression and folding of the PhaC1 constructs (Pfeiffer and Jendrossek, 2011).

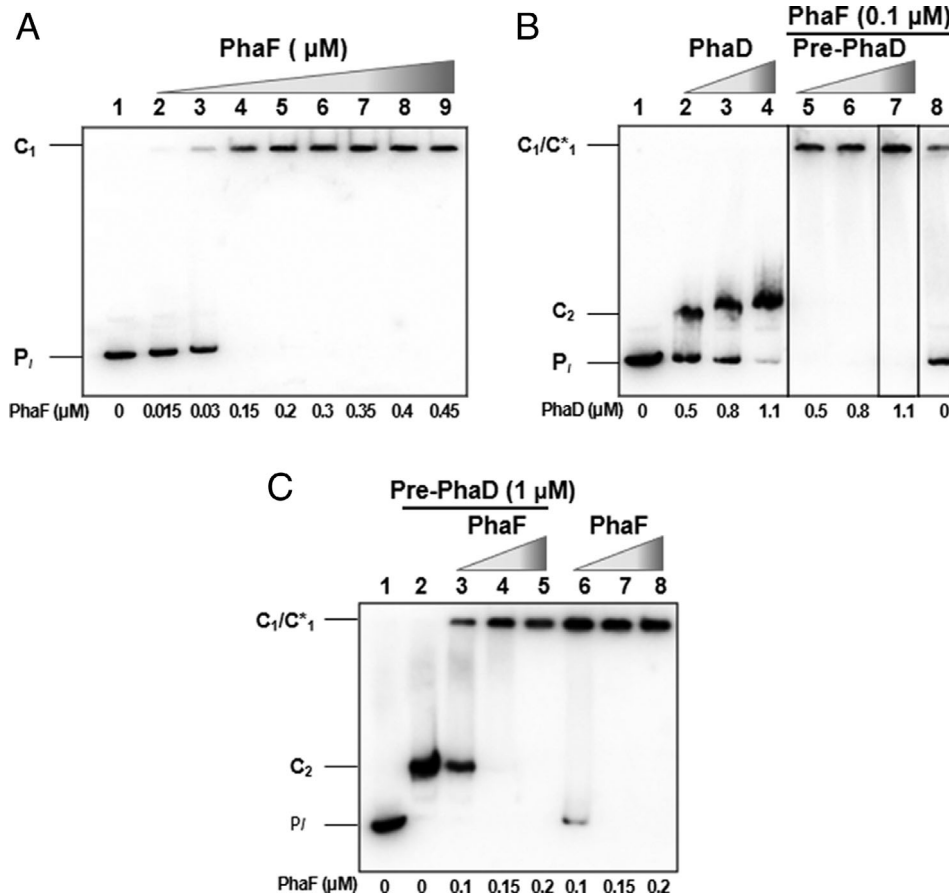
#### *PhaF-PhaD complex formation and DNA binding*

Both PhaF and PhaD are DNA binding proteins involved in the transcriptional regulation of the *pha* cluster. PhaF contains a carboxy-terminal AKP-rich histone-like non-specific DNA-binding domain (Galán *et al.*, 2011; Maestro *et al.*, 2013) and PhaD is a TetR-like activator that binds specifically to its operator at the  $P_{C1}$  and  $P_1$  promoters of the *pha* cluster (de Eugenio *et al.*, 2010). Based on the PD-MS and two-hybrid results indicating

that PhaF and PhaD interact, we wanted to assess their DNA binding capacity when both proteins were present. We performed electrophoretic mobility shift assays (EMSA) with a 230 bp DNA fragment of the promoter  $P_1$  that included the PhaD operator (de Eugenio *et al.*, 2010). Radiolabeled  $P_1$  DNA probe was incubated with increasing concentrations of purified recombinant PhaF (Fig. 6A, lanes 1–9). Notably, concentrations of PhaF higher than 0.03  $\mu$ M saturated probe binding and formed protein-DNA complexes that did not enter the gel (complex  $C_1$ , Fig. 6A, lanes 4–9). Previous work showed that PhaF forms oligomers and predominantly exists as a tetramer in solution (Maestro *et al.*, 2013). It has been proposed that PhaF oligomers could bind along the DNA helix through its basic residues interacting with the phosphate backbone. Thus, in the presence of the  $P_1$  promoter, PhaF could be forming large nucleoprotein complexes that do not enter the gel (complex  $C_1$ ). The binding ability of PhaD to  $P_1$  was also assessed and formed a complex that showed decreased mobility dependent on PhaD concentration (complex  $C_2$ , Fig. 6B, lanes 2–4). At a PhaD concentration above 0.8  $\mu$ M,  $P_1$  was nearly completely bound and retarded by PhaD (complex  $C_2$ ). Although lower concentrations of PhaF were able to form near complete complexes with  $P_1$  when compared to PhaD (starting at 0.15  $\mu$ M vs. 1.1  $\mu$ M, respectively), it was observed that PhaF also retarded a 170 bp DNA fragment from the coding region of the *glpK* gene (Supplemental Fig. S2, lanes 5–7). This demonstrated that PhaF binds to DNA independent of sequence, as was found previously (Galán *et al.*, 2011). PhaD failed to bind to the *glpK* probe due to the specificity of PhaD for its cognate  $P_1$  operator (Supplemental Fig. S2, lanes 2–4).

The interaction between PhaF and PhaD and its effect on DNA binding was further assessed by EMSA experiments. First, the  $P_1$  probe was pre-incubated with different concentrations of PhaD (0.5–1.1  $\mu$ M range) for 10 min (Fig. 6B, lanes 2–4), then a fixed concentration of PhaF (0.1  $\mu$ M) was added to the PhaD- $P_1$  pre-incubated samples (Fig. 6B, lanes 5–7). This resulted in a single complex ( $C^*_1$ ) that did not enter the gel as seen with the  $C_1$  PhaF- $P_1$  complex (compare Fig. 6A, lanes 4–9 and Fig. 6B, lanes 5–7). Thus, even with pre-binding of PhaD to  $P_1$  at concentrations of PhaD that nearly saturated probe binding, only a single complex  $C^*_1$  was observed, equivalent to the PhaF- $P_1$   $C_1$  complex. Whether PhaD definitively formed part of the non-migrating complex  $C^*_1$  could not be demonstrated by this assay. However, the result strongly supported that the presence of PhaF affected the ability of PhaD to unilaterally bind  $P_1$ .

The finding that PhaF forms complexes with  $P_1$  despite PhaD pre-incubation prompted us to investigate if there was a specific concentration of PhaF that would



**Fig. 6.** Electrophoretic mobility shift assay of PhaF and PhaD interacting with promoter  $P_1$ . Native polyacrylamide gels of radiolabeled  $P_1$  DNA probe (1 nM) incubated with (A) increasing concentrations of purified PhaF (lanes 2–9, 0.015–0.45 μM).

B. PI probe preincubated with 0.5–1.1 μM PhaD (lanes 2–4 or 5–7), and further mixed with 0.1 μM PhaF (lanes 5–7). PI incubated with 0.1 μM PhaF without the addition of PhaD (lane 8). C) PI probe preincubated with a fixed 1 μM concentration of PhaD (lanes 2–5) or buffer (lanes 6–8), and further mixed with increasing concentrations of PhaF (lanes 3–5 or 6–8, 0.1–0.2 μM). Vertical lines within panels indicate that lanes were composited. [Color figure can be viewed at [wileyonlinelibrary.com](http://wileyonlinelibrary.com)]

be sufficient to overcome PhaD pre-binding. Therefore, a second experiment was carried out using a fixed concentration of PhaD (1 μM) pre-incubated with  $P_1$  probe, then mixed with increasing concentrations of PhaF (0.1–0.2 μM range, Fig. 6C). Complex  $C_2$  was clearly formed from pre-incubation with PhaD (Fig. 5C, lane 2). However, the PhaD- $P_1$  complex  $C_2$  disappeared with increasing concentrations of PhaF (Fig. 6C, lanes 3–5). The disappearance of complex  $C_2$  was completely replaced by a non-migrating complex equivalent to  $C_1$ , or  $C_1^*$  containing PhaD, at a concentration of 0.15 μM PhaF. In addition, pre-incubation of PhaF and  $P_1$  without incubation with PhaD yielded the  $C_1$  complex (Fig. 6C, lanes 6–8).

Further investigations are required to explore the formation of a PhaF-PhaD- $P_1$  supercomplex, or the possibility that other complexes form that include additional partners (e.g. Phal or PHA granule, forming a PHAgranule-Phal-PhaF-PhaD- $P_1$  supercomplex). Our results confirmed that the presence of PhaF affected the formation of a single PhaD- $P_1$  complex.

## Discussion

### *PhaD as a PhaF interacting partner*

Phasin PhaF has many properties and functions. Structural modelling and experimental data support that PhaF contains at least three separate motifs (Galán *et al.*, 2011; Tarazona *et al.*, 2019a). Its amino terminal region contains the amphipathic alpha-helical structure likely responsible for interacting with PHA. The central core of PhaF contains a leucine zipper motif responsible for its homo- and hetero-oligomerization with the other phasin present in *P. putida*, Phal. Finally, the PhaF carboxy terminal contains a motif capable of binding double stranded DNA in a sequence non-specific manner (Galán *et al.*, 2011; Maestro *et al.*, 2013). Taken together, these results support a model by which PhaF could serve as a bridge between PHA granules and the nucleoid, an interaction that is posited to be responsible for the segregation of PHA granules into both daughter cells during cell division, although other participating partners cannot be excluded. The results presented here build upon and extend the functions of PhaF to include an unpredicted



interaction with the transcriptional regulator of the *pha* locus, PhaD.

The determination of PhaF interacting partners by PD-MS revealed that PhaF interacts with Phal and PhaD, as well as several other proteins (Table 1). Despite PHA-depleted soluble fractions being used as the source of interacting proteins, the presence of Phal in the western blot can be expected as Phal is one of the most abundant proteins produced during PHA accumulating conditions (de Eugenio *et al.*, 2010). Additionally, the interaction between PhaF and Phal was proven to be robust, meaning that PhaF could recruit even small amounts of Phal that detached from PHA granules during sample preparation (Tarazona *et al.*, 2019a). The identification of PhaD in the PhaF PD-MS experiments was strengthened by analysis of the detected PhaD peptides. Peptides identified from PhaD gave a combined coverage of 47% across the three replicates, which likely represent the entirety of possibly detectable peptides considering the limitations of discerning excessively low or high mass peptides (Supplemental Fig. S3). The interaction of PhaF with PhaD revealed a previously unknown association between these two proteins that correlated with the observation that transcription of the *pha* locus was altered in a  $\Delta phaF$  strain (Galán *et al.*, 2011). The two-hybrid results further revealed that there was a direct interaction between PhaF and PhaD not mediated by a third protein (Fig. 5). Remarkably, determination of the PHA granule GAP proteome failed to identify PhaD using two different methods to purify granules (Supplemental Table S1). This result was further supported by microscopic studies revealing that PhaD did not colocalize with granules and instead was found unevenly distributed throughout the cytoplasm (Fig. 4). While further study would be required to determine what this uneven localization pattern represented, it was similar to the organization of nucleoid and ribosomes in PHA producing cells (Kim *et al.*, 2019). Further exploring the roles of both PhaF and PhaD in DNA binding, EMSA results showed that both proteins are capable of binding the  $P_I$  promoter to yield complexes  $C_1$  and  $C_2$ , respectively (Fig. 6A, B). However, binding assays with the addition of increasing amounts PhaF into  $P_I$ -prebound PhaD indicated that PhaF was capable of binding  $P_I$  at the expense of the  $C_2$  complex, forming complexes  $C_1/C^*_1$  (Fig. 6B). Our results could not determine the differences between complexes  $C_1/C^*_1$ . That is, if the presence of PhaF dislocated PhaD to form complex  $C_1$ , or if PhaD was additionally bound to form complex  $C^*_1$ . Taken together, our findings strongly supported that the presence of PhaF affected the ability of PhaD to unilaterally bind  $P_I$ . To further determine whether an *in vivo* supercomplex is formed that simultaneously comprises all the PhaF partners (PHA granule-Phal-PhaF-PhaD- $P_I$ ), and the physiological factors that

drive its formation, would require deeper *in vivo* and *in vitro* analyses. Nevertheless, our results support a new and unexpected viewpoint in the study of the exclusive regulatory system of the PHA machinery.

#### Determination of PHA granule proteome

Previous studies to determine the PHA granule proteome in other organisms suggested that a high number of proteins detected were experimental artefacts from the granule isolation procedure (Jendrossek and Pfeiffer, 2014; Sznajder *et al.*, 2015; Narancic *et al.*, 2018). In fact, a number of dubious proteins were detected in our study using either of the granule isolation methodologies employed. Proteins detected mostly included abundant cellular constituents classified as ATPase subunits, proteins involved in transcription and translation, cell periphery, transport and outer membrane proteins, and protein folding-associated proteins or chaperones (Supplemental Table S1). The enrichment of some of these proteins is explained by the bacterial response to environmental stress, for example, through posttranslational modifications of translation factors (Talavera *et al.*, 2018). For instance, a significant production of elongation factor Tu has been observed in the stationary phase of *P. putida* during PHA accumulation (Mozejko-Ciesielska and Serafim, 2019). This also applies for transport proteins, which are essential for bacteria to maintain an off-equilibrium condition (Wilkins, 2015). Therefore, the identification of these proteins associated with PHA granules might be the result of contamination from other cellular locations (Grünberg *et al.*, 2004; Jendrossek and Pfeiffer, 2014). The detection of proteins such as GroL (Q88N55), Tig (Q88KJ1) and DnaK (Q88DU2) on the surface of the granule is not surprising, since an increase in abundance of some chaperone proteins has been found during nitrogen-limited growth in *P. putida* (Poblete-Castro *et al.*, 2012; Mozejko-Ciesielska and Serafim, 2019). Interestingly, these proteins have also been detected in PHA granules of phasin mutant strains and non-natural PHA-producers where they are proposed to have similar functions as phasins, for example, enhancing protein folding (Pötter *et al.*, 2004; Han *et al.*, 2006). Whether these proteins are specifically bound to the granule surface or represent contamination during the granule preparation has not been determined. Equally interesting was the identification of ATP synthase subunit beta (Q88BX4), flavoprotein-ubiquinone oxidoreductase (a putative electron transfer protein, Q88F95), and the outer membrane protein OprF (Q88L46), in both the PHA granule proteome and the PhaF PD-MS (highlighted in blue in Supplemental Table S1). However, *in silico* analyses of these identified proteins provided no support for interacting with PhaF or their abundance in

**Table 2.** List of strains and plasmids.

Strain/plasmid	Description	Source/Reference
<b>Strains</b>		
<i>E. coli</i> DH10B	Cloning strain	Invitrogen
<i>E. coli</i> JM109	Cloning strain	Stratagene
<i>E. coli</i> BTH101	Adenylate cyclase ( <i>Cya</i> -) deficient strain for bacterial two-hybrid assays	Euromedex
<i>E. coli</i> M15 [pREP4]	Transformation strain for His <sub>6</sub> -protein expression from the pQE32 plasmid; contains pREP4, Km <sup>r</sup>	Qiagen
<i>E. coli</i> BL21 (DE3)	Strain for PhaD expression from the pET29a(+) plasmid; deficient in <i>lon</i> and <i>ompT</i> proteases	Novagen
<i>P. putida</i> KT2440-G	KT2440 derivative strain containing pSEVA238- <i>gfp</i>	This work
<i>P. putida</i> KT2440-IG	KT2440 derivative strain containing pSEVA238-IG ( <i>phal-gfp</i> fusion)	This work
<i>P. putida</i> KT2440-DG	KT2440 derivative strain containing pSEVA238-DG ( <i>phaD-gfp</i> fusion)	This work
<b>Plasmids</b>		
pQE32	His <sub>6</sub> expression vector, Amp <sup>r</sup>	Qiagen
pQE32- <i>phaF</i>	Plasmid for expression of His <sub>6</sub> -PhaF	This work
pET29a(+)	Recombinant protein expression vector, Km <sup>r</sup>	Novagen
pETD	Derivative of pET29a(+) for expression of PhaD-His <sub>6</sub>	This work
pUT18C- <i>phaF</i>	<i>phaF</i> cloned into pUT18C	(Tarazona <i>et al.</i> , 2019a)
pKT25- <i>phaF</i>	<i>phaF</i> cloned into pKT25	(Tarazona <i>et al.</i> , 2019a)
pUT18C- <i>phal</i>	<i>phal</i> cloned into pUT18C	(Tarazona <i>et al.</i> , 2019a)
pUT18C- <i>phaD</i>	<i>phaD</i> cloned into pUT18C	This work
pUT18C- <i>phaC1</i>	<i>phaC1</i> cloned into pUT18C	This work
pKT25- <i>phaC1</i>	<i>phaC1</i> cloned into pKT25	This work
pSEVA238-GFP	Derivative of pSEVA238 containing <i>gfp</i>	Prieto lab
pSEVA238-IG	pSEVA238-GFP derivative containing <i>phal-gfp</i>	This work
pSEVA238-DG	pSEVA238-GFP derivative containing <i>phaD-gfp</i>	This work

Km<sup>r</sup>, kanamycin resistance; Amp<sup>r</sup>, ampicillin resistance.

the PHA granule proteome. Searches using BLASTP for similarity with phasins or MARCOIL for prediction of coiled-coil motifs failed to reveal the presence of any features commonly found in PHA binding proteins. A schematic overview of the GAPs, putative GAPs and PhaD is shown in Fig. S5.

In regards to the detection of proteins directly related to fatty acid and PHA metabolism, the finding that FabG (3-ketoacyl acyl-ACP reductase, Q88QB3) associated with PHA granules is of special interest. In an *E. coli* recombinant strain, this enzyme was shown to convert 3-ketoacyl-CoA into 3HA-CoA monomers that are incorporated into PHA polymers by heterologously expressed PhaC (Ren *et al.*, 2000). This finding suggests that FabG should be further investigated as a GAP.

#### Biological roles of PhaF

Our results support two disparate functions for PhaF when associated with Phal or PhaD. PhaF is associated with Phal on the surface of granules and is additionally associated with PhaD, which is definitively not located on

PHA granules. Our results provide further confirmation of the many functions of PhaF. PhaF has a structural role, in that it interacts with Phal and is involved with the stabilization of PHA granules; a role in granule segregation, to assure proper granule partitioning during cell division; and a regulatory role, in that it interacts with PhaD and is somehow involved with the regulation of transcription of the *pha* locus. PhaF could be involved in regulating transcription through two non-exclusive mechanisms. One mechanism is through the sequence non-specific binding of PhaF to DNA, whereby PhaF works with other regulatory factors for binding to the *pha* promoters. A second mechanism is that PhaF binds to PhaD and modulates the ability of PhaD to exert its function.

The latter mechanism could be related to that of the TetR-family regulator, DhaS, a transcriptional activator of the *dha* operon required for glycerol catabolism in *Lactococcus lactis* (Christen *et al.*, 2006). In contrast to the negative regulation of gene expression observed for most members of the TetR family, DhaS forms a complex with its coactivator DhaQ that in the presence of dihydroxyacetone activates transcription of the *dha* operon.

The binding of dihydroxyacetone to DhaQ in the complex is proposed to induce a conformational change in DhaS, leading to enhanced RNA polymerase recruitment. The interaction of PhaF-PhaD may constitute a similar system as positive regulators of the *pha* operon, and that PhaF may be a coactivator of PhaD. In this sense, a ligand for PhaD has not been determined but it is proposed that intermediates of fatty acid  $\beta$ -oxidation that are PHA precursors may function as inducers of the regulatory system (de Eugenio *et al.*, 2010).

Our results provide new insights into the multiple roles of PhaF, functioning with PhaD bound to DNA and associated with PHA granules along with phasin Phal. This dynamic behaviour highlights how both PHA granule segregation and the proper transcription of the *pha* operon can be accomplished.

## Experimental procedures

### Bacterial strains, media and growth conditions

The strains and plasmids used in this study are listed in Table 2. Unless otherwise stated *Escherichia coli* and *Pseudomonas putida* KT2440 strains were grown aerobically in lysogeny broth (LB) or LB agar at 37 °C and 30 °C, respectively. The media was supplemented, when appropriate, with 100  $\mu$ g/ml ampicillin, 50  $\mu$ g/ml kanamycin or 5  $\mu$ g/ml tetracycline. *E. coli* JM109 was used in the cloning steps for protein purification. *E. coli* M15 [pREP4] was used for the high-level expression of recombinant His<sub>6</sub>-tagged proteins using the pQE32 plasmid. *E. coli* DH10B was used as the cloning strain for the bacterial two-hybrid tests and the GFP-fusions. Bacterial two-hybrid screening assays were performed with the reporter strain *E. coli* BTH101 (Cya<sup>-</sup>, adenylate cyclase deficient) harbouring the pUT18C and pKT25 plasmid combination on LB-X-gal indicator plates containing 100  $\mu$ g/ml ampicillin, 50  $\mu$ g/ml kanamycin, 0.5 mM isopropyl- $\beta$ -D-thiogalactopyranoside (IPTG) and 40  $\mu$ g/ml 5-bromo-4-chloro-3-indolyl- $\beta$ -D-galactopyranoside (X-gal). For PHA accumulation, *P. putida* strains were pre-cultured in LB medium at 30 °C and 200 rpm; overnight growths were washed, transferred to a final OD<sub>600</sub> 0.3 in M63 0.1 N medium, and grown at 30 °C and 200 rpm as previously described (Moldes *et al.*, 2004). M63 0.1 N is a nitrogen limited minimal medium composed of 13.6 g/l KH<sub>2</sub>PO<sub>4</sub>, 0.2 g/l (NH<sub>4</sub>)<sub>2</sub>SO<sub>4</sub>, 0.5 mg/l FeSO<sub>4</sub>·7H<sub>2</sub>O, 1 mM MgSO<sub>4</sub> and a solution of trace elements (composition 1000X per litre: 2.78 g FeSO<sub>4</sub>·7H<sub>2</sub>O, 1.98 g MnCl<sub>2</sub>·4H<sub>2</sub>O, 2.81 g CoSO<sub>4</sub>·7H<sub>2</sub>O, 1.47 g CaCl<sub>2</sub>·2H<sub>2</sub>O, 0.17 g CuCl<sub>2</sub>·2H<sub>2</sub>O, and 0.29 g ZnSO<sub>4</sub>·7H<sub>2</sub>O). Fifteen millimolars of sodium octanoate was used as carbon source for PHA production. Protein extracts for pull-down experiments were obtained from *P. putida* growing on M63

0.1 N for 24 h. Cultures of *P. putida* strains carrying pSEVA238 plasmids (GFP-fusion constructs) were induced with 0.5 mM 3-methylbenzoate.

### Purification of His<sub>6</sub>-tagged proteins

The universal vector pQE32, which allows the production of an amino-terminal His<sub>6</sub>-tagged protein under the control of the T5 promoter, was used to produce recombinant His<sub>6</sub>-PhaF. The 786 bp DNA fragment encoding PhaF was PCR-generated using oligonucleotides 1 and 2 (Supplemental Table S2) and cloned into the pQE32 vector using the BamHI and HindIII restriction enzymes to generate the plasmid pQE32-*phaF*. Overproduction of the His<sub>6</sub>-PhaF protein was achieved in recombinant *E. coli* M15 [pREP4] harbouring pQE32-*phaF* by induction with 1 mM IPTG and subsequent incubation for 16 h at 18 °C to minimize the formation of inclusion bodies. The universal vector pET29a(+), which allows the production of a C-terminal His<sub>6</sub>-tagged protein with a thrombin cleavage site was used for PhaD-His<sub>6</sub> construction. The 615 bp DNA fragment encoding PhaD was PCR generated using the oligonucleotides 3 and 4 in Supplemental Table S2, and cloned into the pET29a(+) vector using the NdeI and KpnI restriction enzymes to create the plasmid pET-*phaD*. Overproduction of PhaD-His<sub>6</sub> was achieved in recombinant *E. coli* BL21 (DE3) harbouring pET-*phaD* by induction with 1 mM IPTG at OD<sub>600</sub> 0.5 and subsequent incubation for 3 h at 37 °C. Protein purifications were carried out as described previously (Tarazona *et al.*, 2019a). Briefly, His<sub>6</sub>-PhaF and PhaD-His<sub>6</sub> were purified from the soluble lysate by metal ion affinity chromatography (IMAC) using an ÄKTA chromatography system (GE Healthcare Life Sciences). The lysates were passed through a column packed with 5 ml of affinity medium Ni-Sepharose (GE Healthcare Life Sciences) charged with NiSO<sub>4</sub> and equilibrated with 50 ml of buffer A (20 mM sodium phosphate pH 7.4, 300 mM NaCl, 30 mM imidazole, 0.1% Triton X-100, and 1 tablet of Roche cComplete™ protease inhibitor cocktail per 50 ml of solution). The column was washed with 25 ml of buffer A and then with 75 ml of a three-step gradient with 5%, 10% and 20% of buffer B (20 mM sodium phosphate pH 7.4, 300 mM NaCl, 500 mM imidazole). A final concentration of 265 and 210 mM of imidazole (50% of buffer B) was used to elute His<sub>6</sub>-PhaF and PhaD-His<sub>6</sub> from the columns, respectively. Fractions were pooled, dialyzed against 150 mM Tris-HCl pH 7.5 and 300 mM NaCl, and concentrated using Amicon® Ultra 15 ml Centrifugal Filters (Merck) with a nominal molecular weight cut-off of 10,000 kDa. Protein concentration was measured by absorbance at 280 nm. Protein molar concentrations were obtained by using the molar extinction coefficients ( $\epsilon_{280}$ ), PhaF = 19,480 M<sup>-1</sup> cm<sup>-1</sup>

and PhaD =  $15,930 \text{ M}^{-1} \text{ cm}^{-1}$ . Protein purity was analysed by 12.5% SDS-PAGE (Supplemental Fig. S4).

#### Affinity purification chromatography: pull-down assays

To identify interacting partners of PhaF, an affinity pull-down followed by mass spectrometry (PD-MS) approach was used. Our method involves (i) incubation of 100  $\mu\text{g}$  of purified His<sub>6</sub>-PhaF (the bait) with *P. putida* cell lysates containing putative interacting proteins, (ii) binding of His<sub>6</sub>-PhaF incubated with lysate to a Ni-Sepharose affinity column, (iii) washing to remove nonspecifically bound proteins, (iv) elution of the bound protein complexes with imidazole and (v) analysis by SDS-PAGE and MS. Recombinant His<sub>6</sub>-PhaF bait protein was expressed and purified as described above, and resuspended in buffer A (20 mM sodium phosphate pH 7.4, 300 mM NaCl, 30 mM imidazole). The pool of cellular proteins was prepared as follow. *P. putida* was grown in PHA accumulation conditions. Cells were harvested, resuspended in buffer A supplemented with Roche cOmplete™ protease inhibitor cocktail (1 tablet per 50 ml of solution) and disrupted by three passages through a French pressure cell at 1000 psi. The sample was treated with 0.1 mg/ml DNase I (Turbo DNA-free™, Ambion) for 20 min at room temperature. The soluble protein fraction was separated from PHA granules (used for granule preparation) and cell debris by centrifugation at  $18,000 \times g$  for 30 min. The concentration of total protein was quantified by Bradford assay. For pull-down experiments, 100  $\mu\text{g}$  of purified His<sub>6</sub>-PhaF was incubated with 1 mg of soluble protein lysate on a roller shaker for 1 h with smooth agitation. The sample was passed through a column packed with affinity medium Ni-Sepharose (GE Healthcare Life Sciences) charged with NiSO<sub>4</sub> and washed and eluted as described for the protein purifications. The PhaF-interacting protein complexes were eluted with 265 mM of imidazole. A pull-down with *P. putida* lysate alone (no His<sub>6</sub>-PhaF) was used as a negative control for non-specific binding to the Ni-Sepharose column. All the experiments were performed at least two times with different biological samples. The eluted fractions were analysed by MS. Western blot analysis was performed to detect Phal in the pull-down assay, as a positive control for a known PhaF interacting partner (Tarazona *et al.*, 2019a). The elution fraction containing proteins that co-eluted with PhaF was separated by 15% SDS-PAGE, and transferred to polyvinylidene fluoride (PVDF) membrane. The membrane was blocked with 5% nonfat milk in PBS-T buffer (10 mM sodium phosphate, 0.15 M NaCl and 0.05% Tween-20) for 1 h, washed with PBS-T, and incubated 2 h with anti-Phal rabbit polyclonal antibody (diluted 1:5000 in PBS-T buffer containing 1% nonfat milk) (Dinjaski and Prieto, 2013).

After washing, the membrane was incubated with anti-rabbit IgG horseradish peroxidase secondary antibody (diluted 1:10000 in PBS; NA934, GE Healthcare Life Sciences), and immunoreactive proteins detected using the Amersham ECL system according to the manufacturer's instructions.

#### PHA granule-associated proteome

To determine the PHA granule proteome of *P. putida* two variations on the granule preparation techniques were utilized. The glycerol granule preparations were from culture extracts treated with DNase I, washed twice with 150 mM NaCl and suspended in 15 mM Tris-HCl, pH 8. The suspension was layered on 55% glycerol, followed by centrifugation in a swinging-bucket rotor 1 h at  $10,000 \times g$  (Dinjaski and Prieto, 2013). Separated PHA granules were collected from the density interface and the centrifugation over glycerol was repeated two more times. For comparison, a second preparation technique was carried out with PHA granules isolated over a discontinuous sucrose gradient (0.43 and 0.58 M) in 50 mM Tris-HCl pH 8, as previously described (Moldes *et al.*, 2004). Cell lysate was centrifuged for 3.5 h,  $120,000 \times g$  at 4 °C, the granule fraction was collected, resuspended in 15 mM Tris-HCl, pH 8, centrifuged for 20 min at  $120,000 \times g$  and stored at -20 °C. For this second method, the cell lysate sample was not treated with DNase I prior to granule preparation. The final granule preparations were separated on a 12.5% SDS-PAGE gel and analysed by MS.

#### MALDI-TOF-TOF peptide mass spectrometry

Proteome analysis was performed by the proteomics core facility of the Biological Research Center of the Spanish National Research Council (CIB Margarita Salas-CSIC, Madrid, Spain) as described in detail previously (Cristobo *et al.*, 2011). A preparative 10% SDS-PAGE containing 500  $\mu\text{g}$  of each elution sample (biological replicates) was run approximately 1 cm and stained with the Colloidal Blue Staining Kit (Invitrogen, Thermo Fisher Scientific) for protein visualization and spot picking. The gel section containing the whole protein fraction was cut-off into two slices and subjected to tryptic digestion. The peptide mixture was loaded onto an Acclaim PepMap 100 precolumn with output to an Acclaim PepMap 100 C18 (3  $\mu\text{m}$  particle size, 75  $\mu\text{m}$  inner diameter  $\times$  25 cm length) analytical column eluting directly into the nano-electrospray source (Thermo Fisher Scientific). Samples were analysed with a LTQ-Orbitrap Velos mass spectrometer (Thermo Fisher Scientific). Fragmented ions were detected with a resolving power of up to 60,000. The top 15 most abundant ions in the scan were selected for MS/MS fragmentation. Selected ions were

fragmented by collision-induced dissociation with normalized collision energies of 35%. Spectrums were processed with Discoverer software Version 1.1.1.14 (Thermo Fisher Scientific). Database searching for protein identification was done using Sequest. Peptide matches were validated using the Percolator algorithm, where a peptide-spectrum match (PSM) was considered correct if it achieved a  $q$  value  $<0.01$  (Käll *et al.*, 2007). Pairwise Pearson's  $r$  correlation coefficients were calculated on PSM values for proteins common in all three PD-MS or the granule proteome datasets using R (<http://www.rproject.org/>). The mass spectrometry proteomics data were deposited to the ProteomeXchange Consortium via the PRIDE partner repository with the dataset identifier PXD018787 (Reviewer Username: reviewer30621@ebi.ac.uk Password: QkTYtxIK) (Perez-Riverol *et al.*, 2019).

#### *In vivo* localization of *PhaD-GFP* and *Phal-GFP* fusions

A variant of the vector pSEVA238 (Standard European Vector Assembly platform) which encodes a green fluorescent protein (GFP) was used for the expression of *PhaD-GFP* and *Phal-GFP* fusions in *P. putida*. The expression system consists of the 3-methylbenzoate-responsive XylS transcriptional regulator and its cognate promoter  $P_m$  driving the inducible expression of the GFP fusions. The *phaD* and *phal* fragments were amplified from *P. putida* KT2440 using oligonucleotides 5–8 (Supplemental Table S2), and cloned in-frame to the 5' end of GFP. The resulting plasmids, pSEVA238-DG (*phaD-gfp* fusion) and pSEVA238-IG (*phal-gfp* fusion) were transformed into *P. putida* via electroporation (Choi *et al.*, 2006). For *in vivo* localization studies, cells carrying the *phaD-gfp* or *phal-gfp* fusion plasmids were transferred from an overnight culture to PHA production conditions and were induced after 2 h of growth with 0.5 mM 3-methylbenzoate. GFP fluorescent signal was detected microscopically after 2 h of induction using a Leica AF6000 LX widefield multidimensional microscopy system and processed with Leica LAS AF lite software.

#### Bacterial two-hybrid assay

*In vivo* protein–protein interactions were studied using the Bacterial Adenylate Cyclase Two-Hybrid System as described previously (Euromedex) (Karimova *et al.*, 2000; Tarazona *et al.*, 2019a). The T18 and T25 complementation fragments of the *Bordetella pertussis* adenylate cyclase catalytic domain were fused at their 3' ends to *P. putida* genes using the vectors pUT18C and pKT25 (oligonucleotides 9–20 in Supplemental Table S2). Plasmids pKT25-bait and pUT18C-target

proteins were co-transformed into the *E. coli* BTH101 (*Cya*<sup>−</sup>) reporter strain and quantification of protein–protein interactions was by assessment of  $\beta$ -galactosidase activity in liquid cultures using the Miller assay (Miller, 1972). *E. coli* BTH101 cultures were grown in 5 ml LB in the presence of 0.5 mM IPTG and the appropriate antibiotics at 30 °C without agitation for 24 h (stationary phase). Western blots of *E. coli* whole cell extracts were carried out to ensure expression of each pUT18C-target fusion construct (data not shown). To assess  $\beta$ -galactosidase activity, the liquid cultures were diluted in PM2 assay buffer (Euromedex: 70 mM Na<sub>2</sub>HPO<sub>4</sub>·12H<sub>2</sub>O; 30 mM NaH<sub>2</sub>PO<sub>4</sub>·H<sub>2</sub>O; 1 mM MgSO<sub>4</sub>; 0.2 mM MnSO<sub>4</sub>, pH 7.0; 100 mM  $\beta$ -mercaptoethanol) to a final volume of 1 ml. Permeabilization of the cells was through the addition of 30  $\mu$ l 100% toluene plus 30  $\mu$ l 0.1% SDS. The  $\beta$ -galactosidase activity was assayed at 28 °C using *o*-nitrophenol- $\beta$ -galactoside (0.25 ml of 0.4% ONPG in PM2 buffer without  $\beta$ -mercaptoethanol) as the substrate. The reaction was stopped by the addition of 0.5 ml of 1 M Na<sub>2</sub>CO<sub>3</sub>. The enzymatic activity,  $A$ , in units per millilitre (U/ml) was quantified according using the formula:

$$A = [200 \cdot (OD_{420} - OD_{420} \text{ in control tube / min of incubation}) \cdot \text{dilution factor}]$$

Where OD<sub>420</sub> is the absorbance of *o*-nitrophenol that results from the hydrolysis of ONPG. One unit of enzymatic activity corresponds to 1 nmol of ONPG hydrolyzed per min at 28 °C. The factor 200 in the above formula is the inverse of the absorption coefficient of *o*-nitrophenol, which is 0.005 per nmol/ml at pH 11 (i.e. after addition of Na<sub>2</sub>CO<sub>3</sub>). The enzymatic activity was finally expressed as units per milligram of cell dry weight (U/mg CDW). CDW was determined from the OD<sub>600</sub> value of the bacterial culture, given that 1 ml of culture at OD<sub>600</sub> 1 corresponds to 300  $\mu$ g of CDW (Euromedex). Under routine conditions, when no interaction occurs, the *E. coli* BTH101 strain basally expresses approximately 150 U/mg CDW. When two-hybrid proteins interact,  $\beta$ -galactosidase activity ranges between 700 to 7000 U/mg CDW, depending on the efficiency of the functional complementation. A co-transformant of pKT25-*zip* and pUT18C-*zip* containing a DNA sequence coding for a leucine zipper motif (Gcn4 leucine zipper) was used as a positive control. For statistical analyses the unequal variances *t*-test was used, a  $p$  value of 0.05 was used as the cut-off for significance. If the  $p$  value was less than 0.05, we rejected the null hypothesis and concluded that a significant difference did exist. Such statistically significant differences are indicated in the figures with an asterisk.

### Electrophoretic mobility shift assay

Electrophoretic mobility shift assays (EMSAs) were conducted using purified His<sub>6</sub>-PhaF and PhaD-His<sub>6</sub> and radioisotope labelled (Fig. 6) or unlabeled (Supplemental Fig. S2) DNA fragments. The upstream region of *phaI*, promoter *P<sub>I</sub>*, was amplified by PCR using oligonucleotides p15' and p13' (21 and 22 in Supplemental Table S2) to generate a 230 bp fragment. Oligonucleotide p15' was labelled at the 5'-end with [ $\gamma$ -<sup>32</sup>P]-ATP (PerkinElmer) using T4 polynucleotide kinase (T4 PNK; New England Biolabs). Labelling reactions (25  $\mu$ l) contained 25 pmol of oligonucleotide, 2.5  $\mu$ l of 10X kinase buffer, 50 pmol of [ $\gamma$ -<sup>32</sup>P]-ATP (3000 Ci/mmol; 10 mCi/ml) and 20 units of T4 PNK, and were incubated at 37 °C for 60 min. Afterwards, reactions were incubated for an additional 20 min at 60 °C to inactivate T4 PNK. Non-incorporated nucleotides were removed using Illustra MicroSpin™ G-25 columns (GE Healthcare).

Binding reactions (10  $\mu$ l) were performed with the <sup>32</sup>P-end-labelled or unlabeled DNA fragment (1 nM) and different concentrations of purified PhaD-His<sub>6</sub> (0.5–1.8  $\mu$ M), His<sub>6</sub>-PhaF (0.015–1  $\mu$ M), or a mixture of both proteins in 10 mM Tris-HCl (pH 7.5) and 100 mM NaCl. The reaction mixtures were incubated for 20 min at 4 °C, and loaded onto pre-run native 5% polyacrylamide gels. Free and bound DNAs were separated by electrophoresis in 1X Tris-borate-EDTA buffer (pH 8.3), at 100 V for 90 min, at room temperature. Gels were dried and labelled DNA was visualized by autoradiography or by using the Fujifilm Image Analyser FLA-3000 and Quantity One software (Bio-Rad). For EMSAs using unlabeled DNA (Supplemental Fig. S2) gels were stained with GelRed nucleic acid stain (Biotium). As a non-specific control we used a DNA fragment (177 bp) of the coding region of the housekeeping gene *glpK*, which was amplified by GlpK5' and GlpK3' oligonucleotides (21 and 22 in Supplemental Table S2).

### Acknowledgements

We thank the Proteomics and Genomics Service of CIB-Margarita Salas for excellent technical assistance. This work was supported by the European Union's Horizon 2020 research and innovation program under grant agreement no. 633962 (P4SB), the Community of Madrid (P2013/MIT2807, P2018/NMT4389) and the Spanish Ministry of Science, Innovation and Universities (BIO2017-83448-R). N.A.T. was funded by the Department of Science, Technology and Innovation-Colciencias, Colombia.

### Authors' contributions

N.A.T. and A.M.H.-A. performed the experiments. All authors designed the study, analysed the results and wrote the paper as well as approved the final manuscript.

### References

- Choi, K.H., Kumar, A., and Schweizer, H.P. (2006) A 10-min method for preparation of highly electrocompetent *Pseudomonas aeruginosa* cells: application for DNA fragment transfer between chromosomes and plasmid transformation. *J Microbiol Methods* **64**: 391–397.
- Christen, S., Srinivas, A., Bähler, P., Zeller, A., Pridmore, D., Bieniossek, C., et al. (2006) Regulation of the *dha* operon of *Lactococcus lactis*: a deviation from the rule followed by the TetR family of transcription regulators. *J Biol Chem* **281**: 23129–23137.
- Cristobo, I., Larriba, M.J., Ríos, V.d.I., García, F., Muñoz, A., and Casal, J.I. (2011) Proteomic analysis of 1 $\alpha$ ,25-Dihydroxyvitamin D3 action on human colon cancer cells reveals a link to splicing regulation. *J Proteomics* **75**: 384–397.
- Cuthbertson, L., and Nodwell, J.R. (2013) The TetR family of regulators. *Microbiol Mol Biol Rev* **77**: 440–475.
- Dinjaski, N., and Prieto, M.A. (2013) Swapping of phasin modules to optimize the in vivo immobilization of proteins to medium-chain-length polyhydroxyalkanoate granules in *Pseudomonas putida*. *Biomacromolecules* **14**: 3285–3293.
- de Eugenio, L.I., Garcia, P., Luengo, J.M., Sanz, J.M., Roman, J.S., Garcia, J.L., and Prieto, M.A. (2007) Biochemical evidence that *phaZ* gene encodes a specific intracellular medium chain length polyhydroxyalkanoate depolymerase in *Pseudomonas putida* KT2442: characterization of a paradigmatic enzyme. *J Biol Chem* **282**: 4951–4962.
- de Eugenio, L.I., Galan, B., Escapa, I.F., Maestro, B., Sanz, J.M., Garcia, J.L., and Prieto, M.A. (2010) The PhaD regulator controls the simultaneous expression of the *pha* genes involved in polyhydroxyalkanoate metabolism and turnover in *Pseudomonas putida* KT2442. *Environ Microbiol* **12**: 1591–1603.
- Galán, B., Dinjaski, N., Maestro, B., de Eugenio, L.I., Escapa, I.F., Sanz, J.M., et al. (2011) Nucleoid-associated PhaF phasin drives intracellular location and segregation of polyhydroxyalkanoate granules in *Pseudomonas putida* KT2442. *Mol Microbiol* **79**: 402–418.
- Grünberg, K., Müller, E.-C., Otto, A., Reszka, R., Linder, D., Kube, M., et al. (2004) Biochemical and proteomic analysis of the Magnetosome membrane in *Magnetospirillum gryphiswaldense*. *Appl Environ Microbiol* **70**: 1040–1050.
- Han, M., Park, S.J., Lee, J.W., Min, B., Lee, S.Y., Kim, S., and Yoo, J.S. (2006) Analysis of poly (3-hydroxybutyrate) granule-associated proteome in recombinant *Escherichia coli*. *J Microbiol Biotechnol* **16**: 901.
- Huisman, G.W., Wonink, E., Meima, R., Kazemier, B., Terpstra, P., and Witholt, B. (1991) Metabolism of poly (3-hydroxyalkanoates) (PHAs) by *Pseudomonas oleovorans*. Identification and sequences of genes and function of the encoded proteins in the synthesis and degradation of PHA. *J Biol Chem* **266**: 2191–2198.
- Jendrossek, D. (2009) Polyhydroxyalkanoate granules are complex subcellular organelles (carbonosomes). *J Bacteriol* **191**: 3195–3202.
- Jendrossek, D., and Pfeiffer, D. (2014) New insights in the formation of polyhydroxyalkanoate granules (carbonosomes) and novel functions of poly(3-hydroxybutyrate). *Environ Microbiol* **16**: 2357–2373.

- Käll, L., Canterbury, J.D., Weston, J., Noble, W.S., and MacCoss, M.J. (2007) Semi-supervised learning for peptide identification from shotgun proteomics datasets. *Nat Methods* **4**: 923–925.
- Karimova, G., Ullmann, A., and Ladant, D. (2000) A bacterial two-hybrid system that exploits a cAMP signaling cascade in *Escherichia coli*. *Methods Enzymol* **328**: 59–73.
- Kim, J., Goni-Moreno, A., Calles, B., and de Lorenzo, V. (2019) Spatial organization of the gene expression hardware in *Pseudomonas putida*. *Environ Microbiol* **21**: 1645–1658.
- Kniewel, R., Revelles Lopez, O., and Prieto, M.A. (2019). Biogenesis of Medium-Chain-Length Polyhydroxyalkanoates. *Biogenesis of Fatty Acids, Lipids and Membranes. Handbook of Hydrocarbon and Lipid Microbiology. Biogenesis Fatty Acids Lipids Membranes*: 457–481. Cham, Switzerland: Springer. [https://doi.org/10.1007/978-3-319-50430-8\\_29](https://doi.org/10.1007/978-3-319-50430-8_29).
- Maestro, B., and Sanz, J.M. (2017) Polyhydroxyalkanoate-associated phasins as phylogenetically heterogeneous, multipurpose proteins. *J Microbial Biotechnol* **20**: 1751–17915.
- Maestro, B., Galán, B., Alfonso, C., Rivas, G., Prieto, M.A., and Sanz, J.M. (2013) A new family of intrinsically disordered proteins: structural characterization of the major phasin PhaF from *Pseudomonas putida* KT2440. *PLoS One* **8**: 15.
- Mezzina, M.P., and Pettinari, M.J. (2016) Phasins, multifaceted Polyhydroxyalkanoate granule-associated proteins. *Appl Environ Microbiol* **82**: 5060–5067.
- Miller, J.H. (1972) *Experiments in Molecular Genetics*, New York: Cold Spring Harbor Laboratory.
- Moldes, C., Garcia, P., Garcia, J.L., and Prieto, M.A. (2004) In vivo immobilization of fusion proteins on bioplastics by the novel tag BioF. *Appl Environ Microbiol* **70**: 3205–3212.
- Mozejko-Ciesielska, J., and Serafim, L.S. (2019) Proteomic response of *Pseudomonas putida* KT2440 to dual carbon-phosphorus limitation during mcl-PHAs synthesis. *Biomolecules* **9**(12), 796.
- Narancic, T., Scollica, E., Cagney, G., and O'Connor, K.E. (2018) Three novel proteins co-localise with polyhydroxybutyrate (PHB) granules in *Rhodospirillum rubrum* S1. *Microbiology* **164**: 625–634.
- Perez-Riverol, Y., Csordas, A., Bai, J., Bernal-Llinares, M., Hewapathirana, S., Kundu, D.J., et al. (2019) The PRIDE database and related tools and resources in 2019: improving support for quantification data. *Nucleic Acids Res* **47**: D442–D450.
- Pfeiffer, D., and Jendrossek, D. (2011) Interaction between poly(3-hydroxybutyrate) granule-associated proteins as revealed by two-hybrid analysis and identification of a new phasin in *Ralstonia eutropha* H16. *Microbiology* **157**: 2795–2807.
- Poblete-Castro, I., Escapa, I.F., Jäger, C., Puchalka, J., Lam, C.M.C., Schomburg, D., et al. (2012) The metabolic response of *P. putida* KT2442 producing high levels of polyhydroxyalkanoate under single-and multiple-nutrient-limited growth: highlights from a multi-level omics approach. *Microb Cell Fact* **11**: 34.
- Pötter, M., Müller, H., Reinecke, F., Wieczorek, R., Fricke, F., Bowien, B., et al. (2004) The complex structure of polyhydroxybutyrate (PHB) granules: four orthologous and paralogous phasins occur in *Ralstonia eutropha*. *Microbiology* **150**: 2301–2311.
- Prieto, M.A., Buhler, B., Jung, K., Witholt, B., and Kessler, B. (1999) PhaF, a polyhydroxyalkanoate-granule-associated protein of *Pseudomonas oleovorans* GPO1 involved in the regulatory expression system for *pha* genes. *J Bacteriol* **181**: 858–868.
- Prieto, A., Escapa, I.F., Martinez, V., Dinjaski, N., Herencias, C., de la Pena, F., et al. (2016) A holistic view of polyhydroxyalkanoate metabolism in *Pseudomonas putida*. *Environ Microbiol* **18**: 341–357.
- Rehm, B.H. (2010) Bacterial polymers: biosynthesis, modifications and applications. *Nat Rev Microbiol* **8**: 578–592.
- Ren, Q., Sierro, N., Witholt, B., Kessler, B. (2000). FabG, an NADPH-Dependent 3-Ketoacyl Reductase of *Pseudomonas aeruginosa*, Provides Precursors for Medium-Chain-Length Poly-3-Hydroxyalkanoate Biosynthesis in *Escherichia coli*. *J Bacteriol*, **182**(10), 2978–2981. <http://dx.doi.org/10.1128/jb.182.10.2978-2981.2000>.
- Ruth, K., Roo, G.d., Egli, T., and Ren, Q. (2008) Identification of two acyl-CoA Synthetases from *Pseudomonas putida* GPO1: one is located at the surface of Polyhydroxyalkanoates granules. *Biomacromolecules* **9**: 1652–1659.
- Sznajder, A., Pfeiffer, D., and Jendrossek, D. (2015) Comparative proteome analysis reveals four novel polyhydroxybutyrate (PHB) granule-associated proteins in *Ralstonia eutropha* H16. *Appl Environ Microbiol* **81**: 1847–1858.
- Talavera, A., Hendrix, J., Versees, W., Jurenas, D., Van Nerom, K., Vandenberg, N., et al. (2018) Phosphorylation decelerates conformational dynamics in bacterial translation elongation factors. *Sci Adv* **4**: eaap9714.
- Tarazona, N.A., Maestro, B., Revelles, O., Sanz, J.M., and Prieto, M.A. (2019a) Role of leucine zipper-like motifs in the oligomerization of *Pseudomonas putida* phasins. *Biochim Biophys Acta Gen Subj* **1863**: 362–370.
- Tarazona, N.A., Machatschek, R., Schulz, B., Prieto, M.A., and Lendlein, A. (2019b) Molecular insights into the physical adsorption of amphiphilic protein PhaF onto copolyester surfaces. *Biomacromolecules* **20**: 3242–3252.
- Wieczorek, R., Pries, A., Steinbüchel, A., and Mayer, F. (1995) Analysis of a 24-kilodalton protein associated with the polyhydroxyalkanoic acid granules in *Alcaligenes eutrophus*. *J Bacteriol* **177**: 2425–2435.
- Wilkens, S. (2015) Structure and mechanism of ABC transporters. *F1000Prime Rep* **7**: 14.
- York, G.M., Stubbe, J., and Sinskey, A.J. (2002) The *Ralstonia eutropha* PhaR protein couples synthesis of the PhaP phasin to the presence of polyhydroxybutyrate in cells and promotes polyhydroxybutyrate production. *J Bacteriol* **184**: 59–66.

## Supporting Information

Additional Supporting Information may be found in the online version of this article at the publisher's web-site:

### Appendix S1: Supporting Information